

Anomalous Thermal Diffusivity in Underdoped $\text{YBa}_2\text{Cu}_3\text{O}_{6+x}$

Jiecheng. Zhang,^{1,2} E. M. Levenson-Falk,^{1,2} B. J. Ramshaw,³ D. A. Bonn,^{4,5}
R. Liang,^{4,5} W. N. Hardy,^{4,5} S. A. Hartnoll,¹ and A. Kapitulnik^{1,2,6,7}

¹*Department of Physics, Stanford University, Stanford, CA 94305*

²*Geballe Laboratory for Advanced Materials, Stanford University, Stanford, CA 94305*

³*Mail Stop E536, Los Alamos National Labs, Los Alamos, NM 87545*

⁴*Department of Physics & Astronomy, University of British Columbia, Vancouver, British Columbia, Canada V6T 1Z1*

⁵*Canadian Institute for Advanced Research, Toronto, Ontario, Canada M5G 1Z8*

⁶*Department of Applied Physics, Stanford University, Stanford, CA 94305*

⁷*Stanford Institute for Materials and Energy Sciences, SLAC National Accelerator Laboratory,
2575 Sand Hill Road, Menlo Park, California 94025, USA*

(Dated: February 2, 2022)

The thermal diffusivity in the ab plane of underdoped YBCO crystals is measured by means of a local optical technique in the temperature range of 25 – 300 K. The phase delay between a point heat source and a set of detection points around it allows for high-resolution measurement of the thermal diffusivity and its in-plane anisotropy. Although the magnitude of the diffusivity may suggest that it originates from phonons, its anisotropy is comparable with reported values of the electrical resistivity anisotropy. Furthermore, the anisotropy drops sharply below the charge order transition, again similar to the electrical resistivity anisotropy. Both of these observations suggest that the thermal diffusivity has pronounced electronic as well as phononic character. At the same time, the small electrical and thermal conductivities at high temperatures imply that neither well-defined electron nor phonon quasiparticles are present in this material. We interpret our results through a strongly interacting incoherent electron-phonon “soup” picture characterized by a diffusion constant $D \sim v_B^2 \tau$ where v_B is the soup velocity, and scattering of both electrons and phonons saturates a quantum thermal relaxation time $\tau \sim \hbar/k_B T$.

The standard paradigm for transport in metals relies on the existence of quasiparticles. Electronic quasiparticles conduct electricity and heat. Phonon quasiparticles, the collective excitations of the elastic solid (here, we discuss acoustic phonons) also conduct heat. Transport coefficients, such as electrical and thermal conductivities, can then be calculated using, for example, Boltzmann equations[1]. However, such an approach fails when the quasiparticle mean free paths becomes comparable to the quasiparticle wavelength. For electrons it is the Fermi wavelength [2–4], while for phonons it is the larger of the interatomic distance or minimum excited-phonon wavelength [5, 6]. Understanding transport in non-quasiparticle regimes requires a new framework and has become a subject of intense theoretical effort in recent years triggering an urgent need for experimental results which can shed light on such regimes. In particular, in [7], the diffusivity was singled out as a key observable for incoherent non-quasiparticle transport, possibly subject to fundamental quantum mechanical bounds.

In this letter we report high-resolution measurements of the thermal diffusivity of single crystal underdoped $\text{YBCO}_{6.60}$ (an ortho-II $\text{YBa}_2\text{Cu}_3\text{O}_{6.60}$), and $\text{YBCO}_{6.75}$ (an ortho-III $\text{YBa}_2\text{Cu}_3\text{O}_{6.75}$). We are particularly interested in the anisotropy of the thermal diffusivity as measured along the principal axes a and b (which is the chain direction) in the temperature range 25 to 300 K. We use a non-contact optical microscope to perform local thermal transport measurements on the scale of ~ 10 μm , hence avoiding inhomogeneities, particularly twin-

ning and grain boundary effects. Our principal experimental results are: i) the measured thermal diffusivity is consistent with the previously measured thermal conductivity and specific heat, satisfying $\kappa = cD$. The high-temperature specific heat is known to be dominated by phonons. However, ii) the phonon mean free path implied by the magnitude of the measured diffusivity is of order, or smaller than, the phonon wavelength. In addition: iii) the intrinsic thermal anisotropy is found to be almost identical to the electrical resistivity anisotropy; and iv) the thermal anisotropy starts to decrease rather sharply below the charge order transition.

A complete understanding of transport in the high temperature regime of the YBCO (or similar) material system requires that we interpret our diffusivity results together with previously reported measurements of the charge sector on similar crystals at temperatures above the charge order transition, primarily photoemission spectroscopy [8, 9] and electrical resistivity [10–12]. Those measurements suggest that the electronic mean free path is also comparable or smaller than the electron wavelength, and thus at or beyond the Mott-Ioffe-Regel (MIR) limit [The MIR limit has been expressed in different ways in the literature, e.g. as $k_F \ell \approx 1$ or $\ell/a \approx 1$ (k_F is the Fermi wavevector, a is the lattice constant, and ℓ is the mean free path). These approaches typically produce the same order of magnitude estimate. In this paper we use the criterion proposed in [2] of $\ell/\lambda_F \approx 1$ where $\lambda_F = 2\pi/k_F$]. The simultaneous destruction of phonon and electron quasiparticles, together with com-

parable anisotropies in thermal and charge transport, suggest that scattering is dominated by strong electron-phonon interaction. The lack of coherent response is furthermore incompatible with electron-phonon composite quasiparticles such as polarons [13] or bipolarons [14]. We are therefore led to conjecture a novel type of transport in the YBCO (or similar) system, in the temperature regime where quasiparticles are not well defined, which is dominated by diffusion of an electron-phonon “soup”. Furthermore, all relaxation processes of electrons and phonons, and hence of charge and heat, are saturated at the thermal relaxation time $\tau \sim \hbar/k_B T$. This ‘Plankian’ timescale has previously been proposed to underpin transport across many families of unconventional metals [15–17], and is widely observed in optical data on cuprates [18–21]. A simple model based on the above ansatz shows excellent fit to the temperature dependence of the measured thermal diffusivity using measured material parameters. This approach generalizes the recently proposed incoherent metallic transport [7] to the case where the electronic system exhibits strong interactions with additional degrees of freedom—the phonons. An immediate further generalization of our idea could apply to complex insulators at high fields, with magnetic or polarization excitations playing the role of the phonons.

RESULTS AND DISCUSSION

Thermal Diffusivity Measurements

For the high resolution thermal diffusivity measurements we use a photothermal microscope (see SI - Supplemental Information), where a modulated power of a heating laser beam causes ripples in the temperature profile at the sample surface, which may be measured by a probing laser due to the change in reflectivity as a function of temperature. We obtain the diffusivity D by fitting the phase delay between the source and the response signals as a function of the modulation frequency ω at fixed distance r between the source and probe beam (see Methods). In the case of an anisotropic sample, the extracted diffusivity depends on orientation θ as follows

$$D = \frac{D_a D_b}{D_b \cos^2 \theta + D_a \sin^2 \theta} \quad (1)$$

where D_1 and D_2 are the diffusivities of the two principle axes on the surface. Since $D = \kappa/c$, where the specific heat c is a scalar quantity, the diffusivity inherits its spatial anisotropy from the thermal conductivity tensor κ . Several $\text{YBa}_2\text{Cu}_3\text{O}_{6+x}$ samples were measured; all showed consistent results with the two samples reported here: a detwinned single crystal of $\text{YBCO}_{6.60}$ measuring approximately $3 \text{ mm} \times 2 \text{ mm} \times 1 \text{ mm}$, and a detwinned single crystal of $\text{YBCO}_{6.75}$ measuring approximately $2 \text{ mm} \times 1 \text{ mm} \times 0.4 \text{ mm}$. Fig. S1(c) in SI shows

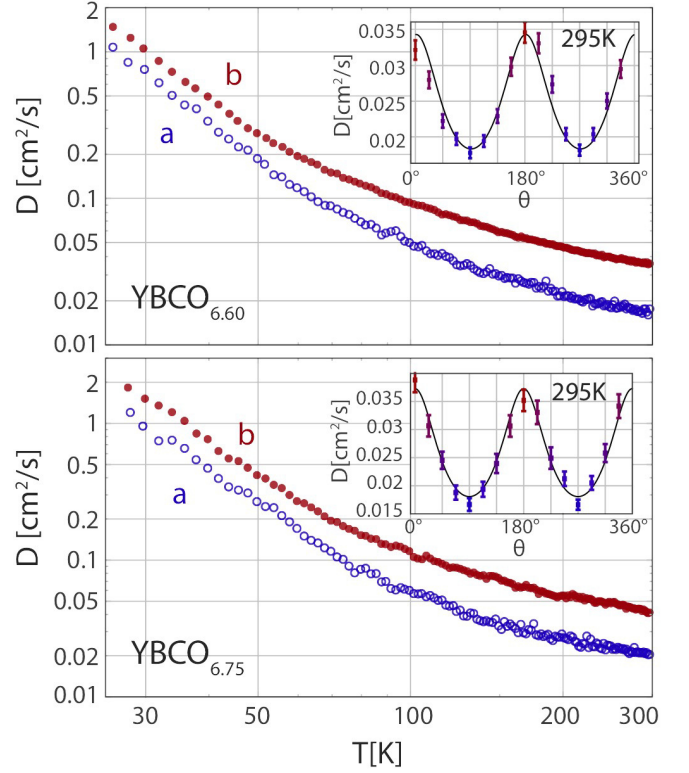


Figure 1. (color online) Thermal diffusivity of $\text{YBCO}_{6.60}$ and $\text{YBCO}_{6.75}$ single crystals, extracted from phase measurement, plotted on a log-log scale as a function of temperature in the range 25 – 300 K. Insets show diffusivity measured at room temperature as a function of orientation around the heating spot, with the solid lines representing fits to Eq. 1 (see text). Error bars are almost entirely due to uncertainty in determining lasers spots separation.

the surface of the $\text{YBCO}_{6.75}$ with the focused laser spots under polarized light, where bright/dark stripes are the twin domains. The small scale of measurement enables us to measure local diffusivity in all directions of the Cu-O planes while avoiding edges, twin boundaries, and other visible defects when possible. At room temperature (RT), both samples have reflectivity $R \approx 0.15$, and $dR/dT \approx 10^{-4} \text{ K}^{-1}$ at 820 nm. The typical power of the probing laser is $\lesssim 0.2 \text{ mW}$, and typical RMS power of the heating laser is $\lesssim 0.5 \text{ mW}$. Using thermal conductivities reported in existing literature [?], we estimate the increase in mean temperature due to both lasers to be less than 1 K in the entire temperature range of interest. To check the alignment of the sample, we first measure diffusivity as a function of sample orientation relative to the axis of displacement of the laser spots, shown in the insets of Fig. 1. Error bars are due to the $\sim 0.5 \mu\text{m}$ uncertainty in determining the distance r between the two spots and thus in extracting D from the data. The solid line is a fit to Eq. 1, showing excellent agreement. The offset angle is left as a free parameter, but agrees with the alignment to the sample edge to within 1° . We

find that the local orientation of the a - and b -axis swap between different twinning domains, verifying the single-domain nature of our measurements. Small variations (of order 10%) in diffusivity are measured at different areas on the sample surface, which we attribute to material inhomogeneity. Once the principal axes are determined from the detailed anisotropy study, the temperature dependence of the diffusivity is measured along each of the principal axes in a continuous temperature sweep at a fixed frequency.

Initial Observations

The temperature dependence of the diffusivities along both the a - and b -axis for the two samples are shown in Fig. 1. We observe that the diffusivity increases at lower temperatures, increasing by almost two orders of magnitude in the temperature range studied here. Using existing measurements of specific heat on similar YBCO crystals [22], we obtain the respective thermal conductivities of the crystals; both show excellent agreement with previously measured thermal conductivities of YBCO crystals with similar doping (e.g. κ_a for YBCO_{6.60} was previously measured by Waske *et al.* and Minami *et al.* [23]). The temperature dependence of the thermal anisotropy, D_a/D_b , for both samples are shown in Fig. 2. Three main features of the data are observed. First, the anisotropies of the two samples are similar. Second, the anisotropy is almost temperature independent with $D_a/D_b \sim 2$ at high temperatures, but decreases sharply below the charge density wave (CDW) transition ($\sim 140 - 150$ K [24]). Third, the size and temperature dependence of the thermal anisotropy are very similar to those of the anisotropy of the electrical resistivity. In Fig. 2 we also plot the resistivity anisotropy of YBCO_{6.75} from ref. [12], measured on very similar crystals. Since the resistivity measures transport of the electronic system, we conclude here that the thermal diffusivity exhibits a strong electronic character. Furthermore, while at low doping levels the charge order is strongly anisotropic (see e.g. [25]), for the YBCO_{6.60} [26] and YBCO_{6.75} [27] reported here, an almost isotropic CDW transition would not strongly affect the diffusivity anisotropy of conventional phonons. Instead, in mirroring the behavior of the electrical resistivity, the decrease in anisotropy again indicates electronic contribution to the thermal diffusivity. The onset of CDW order can both change the scattering mechanism of the electrons and also lead to new collective transport dynamics. The electronic excitations may ultimately regain their quasiparticle character, including possible polaronic behavior [13, 14]. Furthermore, the CDW transition in this material is correlated with a strong electron-phonon interaction [28, 29]. We further elaborate on these points below.

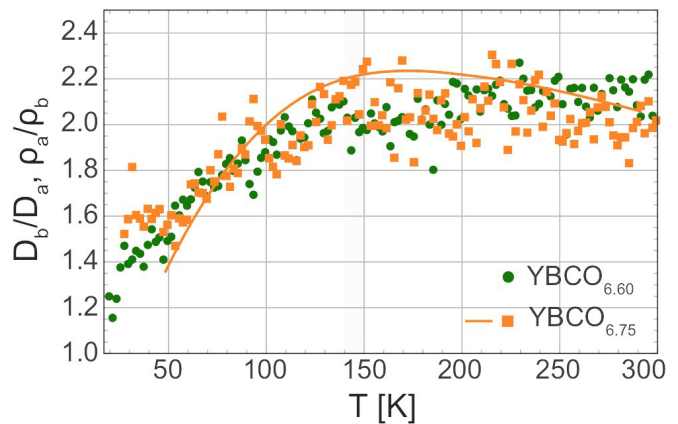


Figure 2. (color online) Anisotropy of the ab -plane thermal diffusivity as a function of temperature of YBCO_{6.60} (green circles) and YBCO_{6.75} (orange squares). Charge density order occurs at around $140 - 150$ K in both materials (see e.g. [24]), marked by the grey region. Note that anisotropies decrease significantly below the transition, signifying the non-trivial role the electronic system plays in the thermal transport. Solid line is the electrical anisotropy in the ab plane on similar crystals adopted from [12].

Good Metals vs. Bad Metals

The conventional treatment of heat conduction in itinerant solids assumes the existence of well defined quasiparticle excitations that transport entropy: electrons and phonons. The mean free paths, ℓ_e and ℓ_{ph} for the electrons and phonons respectively, are assumed to be much larger than their respective wavelength. For electrons to be well defined quasiparticles we require that $\ell_e/\lambda_F \gg 1$, where λ_F is the Fermi wavelength. The limiting case $\ell_e/\lambda_F \sim 1$ is called the Mott-Ioffe-Regel (MIR) limit [?], beyond which the material is dubbed a “bad metal” [2]. Analogously, for well defined phonon excitations we require that $\ell_{ph} \gg \max\{a, \lambda_{min}\}$, where a is the lattice constant and $v_s/\lambda_{min}(T)$ (v_s is the sound velocity) is the highest acoustic phonon frequency excited at temperature T [5, 6]. If both conditions are met, the thermal conductivity of the solid will be the sum of the thermal conductivities of the electrons and phonons, which can also be written as products of the respective diffusivities and specific heat capacities:

$$\kappa = \kappa_e + \kappa_{ph} = c_e D_e + c_{ph} D_{ph} = cD. \quad (2)$$

The last equality states that the measured thermal diffusivity is a heat capacity weighted average of the two diffusivities, and $c = c_e + c_{ph}$.

The consequences of Eqn. 2 are well demonstrated in the case of both good and disordered metals, even at temperatures of order the Debye temperature. Table I gives examples of room temperature (RT) thermal transport parameters for good metals (copper, gold, silver, tungsten), metals with large RT resistivity (mercury, constan-

Metals	D cm ² /s	c J/cm ³ -K	$\kappa^* = cD$ W/cm-K	κ W/cm-K	ρ $\times 10^5 \mu\Omega\text{-cm}$	v_s cm/s	$\kappa_{ph}^{min} \approx cv_s a$ W/cm-K	$\kappa_e(L_0)$ W/cm-K	L/L_0	θ_D K
Copper	1.15 ⁴	3.45 ¹	3.97	3.98 ¹	1.67 ¹	3.56 ¹	0.044	4.4	0.91	310 ²
Gold	1.28 ⁵	2.5 ¹	3.2	3.15 ¹	2.24 ¹	3.25 ¹	0.033	3.3	0.96	185 ²
Silver	1.61 ⁴	2.47 ¹	4.0	4.27 ¹	1.59 ¹	3.6 ¹	0.036	4.6	0.95	220 ²
Tungsten	0.68 ⁶	2.56 ¹	1.74	1.78 ¹	5.65 ¹	5.25 ¹	0.042	1.3	1.27	315 ²
Hg	0.043 ⁷	1.88 ¹	0.081	0.084 ¹	96 ²	1.45 ¹	0.0085	0.074	1.11	110 ²
Constantan	0.064 ⁸	3.65 ²	0.23	0.21 ^{1,2}	49.9 ¹	5.2 ¹	0.07	0.15	1.32	390 ³
Inconel 718	0.029 ²³	3.5 ²	0.101	0.097 ²	156 ²	4.94 ²	0.06	0.05	1.56	410 ³
YBCO _{6.6} (a-dir)	0.016-0.018 ²⁴	2.7 ⁹	0.043-0.05	0.05-0.065 ¹²	560-700 ¹³	6.05 ¹⁸	0.063	0.013	5.0-5.4	410 ¹¹
YBCO _{6.75} (a-dir)	0.018-0.02 ²⁴	2.7 ⁹	0.05-0.054	0.047-0.068 ¹²	430-500 ¹³	6.05 ¹⁸	0.063	0.017	4.1-5.0	410 ¹¹
LSCO(x=0.13)	0.021 ²¹	2.67 ¹⁰	0.056	0.057 ¹⁴	700 ¹⁶	5.9 ¹⁹	0.06	0.01	4.5-5.5	400 ¹⁰
BSCCO:2212	0.021 ²²	2.35 ¹¹	0.048	0.058 ¹⁵	580-780 ¹⁷	4.3 ²⁰	0.055	0.009	4.6-6.2	280 ¹¹

Table I. **Room temperature thermal transport parameters for selected good metals, disordered metals, and cuprates.**

Comparison of room-temperature thermal properties of good metals, disordered metals, and cuprates. LSCO data are for $\text{La}_{1.87}\text{Sr}_{0.13}\text{CuO}_4$ (see Fig. S4). BSCCO data are for optimally doped $\text{Bi}_2\text{Sr}_2\text{CaCu}_2\text{O}_8$ as found in the literature. YBCO_{6.60}(a-dir) and YBCO_{6.75}(a-dir) a-direction data are on single crystals from similar doping, whereas diffusivity data are from this work. Discussions on $\kappa^* = cD$, $\kappa_{ph}^{min} \approx cv_s \ell_{ph}$ (with $\ell_{ph} = a$; a is the lattice constant), and $\kappa(L_0) = L_0 T / \rho =$ are in the text. Superscripts are the references for the quoted data as follows: ¹=^[31]; ²=^[32]; ³=calculated from ^[32]; ⁴=^[30]; ⁵=^[33]; ⁶=^[34]; ⁷=^[35]; ⁸=^[36]; ⁹=^[22, 38]; ¹⁰=^[38]; ¹¹=^[41]; ¹²=^[23, 39]; ¹³=^[10, 12, 23]; ¹⁴=^[42]; ¹⁵=^[6]; ¹⁶=^[43]; ¹⁷=^[46, 47]; ¹⁸=^[40]; ¹⁹=^[44]; ²⁰=^[48]; ²¹=see SI; ²²=^[45]; ²³=^[37]; ²⁴=this work (spread due to inhomogeneity).

tan, Inconel), and several cuprates, which are known to be “bad metals” at RT. In the case of good and disordered metals, ample data is available on identically prepared samples to confirm that at RT the thermal conductivity κ closely matches the measured diffusivity times the measured specific heat (κ^* in Table I). Furthermore, when the electronic thermal conductivity $\kappa_e(L_0)$ is calculated from the resistivity using the Wiedemann-Franz law ($\kappa\rho/T = L$) and the theoretical value of the Lorenz number $L_0 = 2.44 \times 10^{-8} \text{W}\cdot\Omega/\text{K}^2$, the result is very close to the measured thermal conductivity, yielding a measured $L/L_0 \approx 1$.

Unfortunately, not much data is available for the cuprates where the diffusivity, specific heat, thermal conductivity, and resistivity have all been measured on the same sample, or at least on same-doping samples made with the same protocol. For example, a -direction thermal conductivity on YBCO_{6+x} was reported by Minami *et al.* [23], but for similar dopings, their crystals show much larger resistivity than measurements done on crystals similar to ours [12]. At the same time, Inyushkin *et al.* measured twinned crystals with similar doping levels, which are expected to yield a larger value as the a - and b -directions average [49]. We therefore base our estimates on a range of thermal-parameters values as found in the literature.

Analyzing the available data for the cuprates, we first note that also here $\kappa \sim \kappa^*$, but now $\kappa \gg \kappa_e(L_0)$. At the same time we find it to be very close to, and sometimes smaller than, κ_{ph}^{min} . This minimum phonon thermal conductivity is calculated as the product of the sound velocity, the lattice constant and the specific heat, and

amounts to setting $\ell_{ph} = a$ as discussed above. It is a lower bound to the total thermal conductivity of a system with well defined quasiparticles regardless of electron participation (a complementary bound on κ_{ph}^{min} using λ_{min} instead of a is discussed below.) For good metals $\kappa_{ph}^{min} \ll \kappa$, and $L/L_0 \sim 1$ as is expected from electron-dominated thermal transport. Mercury at RT is a liquid with a relatively slow sound velocity. Nevertheless, it shows similar behavior to the best metallic elements with thermal transport dominated by electrons. On the other hand, with increasing resistivity due to disorder, constantan and Inconel show a tendency to a decreased thermal conductivity, and an increasing Lorentz number. The bad metal cuprates on the other hand show at RT $\kappa \approx \kappa_{ph}^{min}$, with anomalously large Lorentz number. These facts might raise doubts on whether high-temperature thermal transport in cuprates has any significant electronic contribution at all, cf. [23], in apparent tension with the electronic character noted in the previous section.

Failure of the Quasiparticle Picture

While at lower temperatures it is believed that quasiparticle excitations are well defined [8, 50], the situation must change close to the MIR limit. Indeed, applying the conventional treatment to our diffusivity measurements in the temperature range $\gtrsim 150$ K raises several problems that challenge the self-consistency of the quasiparticle approach. Within a quasiparticle interpretation, $\kappa_e(L_0) \ll \kappa$, and so we would conclude that

the high-temperature thermal transport is dominated by phonons. Even without assuming quasiparticles, at high temperature the phonon specific heat is overwhelmingly large compared to that of the electrons [22, 51]. Thus, since the product of the specific heat and our measured diffusivity yields the commonly measured thermal conductivity, the naive conclusion is that phonons dominate the high temperature thermal transport, and we should expect to measure $\kappa = cD \approx c_{ph}D_{ph} = \kappa_{ph}$. However, even in this phonon-dominated picture, we see that $\kappa_{ph} \approx \kappa_{ph}^{min}$, and so $\ell_{ph} \approx a$. Since room temperature is well below the Debye temperature for this material, it is appropriate to use a stricter bound on κ_{ph}^{min} associated with λ_{min} (instead of a). Assuming that the highest frequency phonon excited at RT is proportional to temperature, the corresponding minimum phonon wavelength is $\lambda_{min} \sim \hbar v_s / k_B T$. The sound velocities of a similar YBCO_{6.60} crystal have been measured yielding $v_s^a = 6.0 \times 10^3 \text{ m/s}$ and $v_s^b = 6.5 \times 10^3 \text{ m/s}$ [40]. Shear sound velocity may be a factor $\sim \sqrt{3}$ smaller, which does not change the following arguments. Note that these velocities (along with the lattice constants) would yield a much more isotropic diffusivity than the measured D . Assuming now two-dimensional phonon transport, the “classical” phonon diffusivity satisfies $D_{ph} = v_s \ell_{ph} / 2$, and thus we estimate $\ell_{ph} / \lambda_{min} \approx 2Dk_B T / \hbar v_s^2 \sim 0.6 < 1$ (for D_a at RT), violating the condition for well defined phonon excitations. A similar analysis was previously reported by Allen *et al.* [6] on Bi₂Sr₂CaCu₂O₈ single crystals, concluding that phonons are poorly defined in this system. However, their treatment of the electronic contribution relied on a standard application of the WF law, which was subsequently shown by Zhang *et al.* [52] to fail around RT. Finally we note that (see table I) the values of a -direction D for the YBCO_{6+x} crystals is practically the same as the values for the more isotropic (in the Cu-O planes) cuprates. Similar observations can be found for the resistivity of the cuprates (e.g. b -axes resistivities can be found in [10, 12]). This must indicate that the chains have excess electronic conduction rather than phononic one.

The phonon quasiparticle approach is therefore not consistent. Likewise for the electrons, examination of the resistivity data for similar crystals at around RT yields $\ell_e / \lambda_F \sim 1$ (see e.g. [10, 12]). Beyond the short mean free paths, the phonon dominance suggested by a quasiparticle interpretation is incompatible with the fact that our measured diffusivity anisotropy is similar to the electrical resistivity anisotropy, and sensitive to the onset of charge order at ~ 150 K. We are led to conclude that *thermal transport has strong electronic in addition to phononic character, with no simple way to separate them*, especially in view of the typically very strong electron-phonon interaction in the cuprates [9].

The Case for an Incoherent Electron-Phonon “Soup”

We are therefore led to propose a new approach to transport in strongly interacting systems where neither elementary excitations are well defined. Without quasiparticles, including the absence of emergent well-defined electronic excitations (e.g. collective modes related to a possible symmetry breaking, or dressed coherent excitations such as polarons and bipolarons), the mean free path has no meaning. However, microscopic relaxation timescales can still be defined. Following [7], we conjecture that all microscopic degrees of freedom, electronic or phononic, saturate a (momentum non-conserving) relaxation bound leading to overdamped diffusive transport with quantum thermal timescales $\tau \propto \hbar / k_B T$. The resulting diffusion coefficient is connected to the thermal timescale through a (temperature dependent) effective velocity, $v_B(T)$, such that

$$D = \frac{1}{2} v_B(T)^2 \frac{\hbar}{k_B T} \quad (3)$$

where the factor of 2 represents the quasi two-dimensional diffusion in the Cu-O planes. This approach suggests that in the strongly coupled, high temperature limit the electron-phonon system behaves as a composite, strongly correlated “soup” with an effective velocity v_B . This velocity is expected to lie between the faster Fermi velocity of the electrons and the much slower sound velocity of the phonons: $v_s < v_B < v_F$.

To obtain an estimate of v_B , we may attempt to extrapolate the expression for the thermal conductivity from the regime where quasiparticles are well defined and equation (2) holds

$$\kappa = cD = c_e \left(\frac{1}{2} v_F^2 \tau_e \right) + c_{ph} \left(\frac{1}{2} v_s^2 \tau_{ph} \right) \quad (4)$$

to the new strongly coupled regime. Assuming a smooth interpolation between the two regimes, we bound the electron and phonon relaxation times in the above equation by

$$\tau_{ph} = \alpha_{ph} \frac{\hbar}{k_B T}, \quad \text{and} \quad \tau_e = \alpha_e \frac{\hbar}{k_B T} \quad (5)$$

where α_{ph} and α_e are numerical constants of order unity. The resulting expression for the diffusivity is

$$D = \frac{\hbar}{2k_B T} \left(\alpha_e \frac{c_e}{c} v_F^2 + \alpha_{ph} \frac{c_{ph}}{c} v_s^2 \right). \quad (6)$$

Equation (6) now has the form (3) with $v_B = \bar{v}_B(T)$, where

$$\bar{v}_B(T)^2 = \alpha_e \frac{c_e}{c} v_F^2 + \alpha_{ph} \frac{c_{ph}}{c} v_s^2, \quad (7)$$

which clearly satisfies the condition $v_s < \bar{v}_B < v_F$ (we note that, in the expression for the thermal conductivity,

only the heat capacity associated with the modes that propagate in the measured direction and carry entropy should be included. However, this difference may only change the expression by a factor of order unity). More generally one would like to identify v_B with a universally defined non-quasiparticle velocity. It has been noted [53] that in some non-quasiparticle systems it is the “butterfly velocity” [54, 55] that appears in the diffusivity formula 3.

Fig. 3 shows the temperature dependence of D^{-1} with the fit to Eqn. (6) above 150K, where we are free of the interference with the onset of charge order [26, 27]. Using the known temperature dependent total heat capacity [22] and electronic specific heat [56] (at RT $c_{ph} \sim c$ while $c_e \sim 0.014c$), and assuming in-plane Fermi velocity found e.g. in ARPES measurements $v_F \approx 2.15 \times 10^7$ cm/sec [57], we find e.g. for YBCO_{6.75} that in the Cu-O planes the prefactor $\alpha_e \approx 0.25 \pm 0.02$, and $\alpha_{ph} \approx 1.64 \pm 0.09$, while along the chains $\alpha_e \approx 0.53 \pm 0.02$, and $\alpha_{ph} \approx 2.8 \pm 0.2$. Hence the temperature dependent microscopic velocity \bar{v}_B , defined in Eqn. (7), exhibits significant character of both electrons and phonons with similar coefficients of order unity and velocity $v_s < \bar{v}_B < v_F$. The small errors associated with the coefficients (see Supporting Information (SI)) signal the robustness of the fit, while the independently measured temperature dependences of c_e and c_{ph} are responsible for the curvature away from $D^{-1} \propto T$ in the figure. Furthermore, signatures of an electron-phonon soup are seen in the behavior of the electrical resistivity, which is not exactly T -linear over our temperature range. Comparing our diffusivity data with existing electrical resistivity measurements [10, 12] shows that in the bad metal regime $d\rho/dT \propto d(D^{-1})/dT$, implying that the sound speed contributes to the electrical resistivity.

The above analysis yields a novel transport mechanism for strongly interacting systems that exceed the quasiparticle mean free path limit. Thermal transport proceeds by collective diffusion of a composite electron-phonon “soup”, which is distinct from any system exhibiting well defined electron-phonon quasiparticles such as polarons or bipolarons [13, 14]. Entropy diffusion is characterized by thermal timescales and a unique velocity. Consequently, commonly used electronic-transport characteristics, such as e.g. the Wiedemann-Franz law, are not well-defined in this regime. In the YBCO cuprates this scenario seems to persist down to the charge order temperatures, below which electrons presumably start to regain their quasiparticle character and hence decouple from the electron-phonon “soup.” Obviously, a main ingredient of this scenario is the strong electron-phonon interaction which in turn may have some impact on the high T_c found in the cuprates.

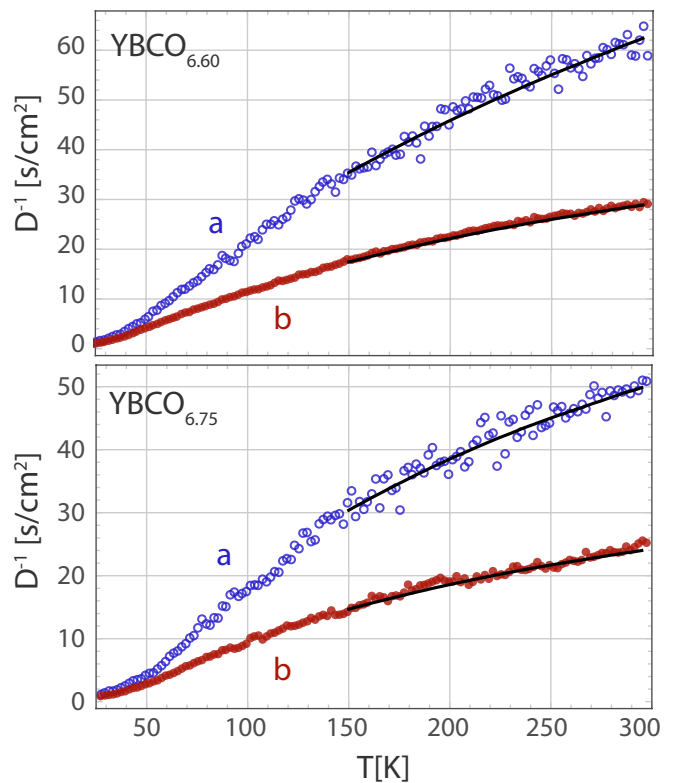


Figure 3. (color online) Inverse diffusivity along the a - (unfilled blue circles) and b -axis (filled red circles) for both materials. The solid lines are fits to Eq. 6 (see text.)

Conclusions

In conclusion, we have shown that the underdoped YBa₂Cu₃O_{6+x} system, above the charge order transition, exhibits anomalous thermal transport. Neither the phonons nor the electrons are well defined quasiparticles, while their strong mutual interactions cause both to saturate the relaxation timescale at $\sim \hbar/k_B T$. This results in a unique type of heat transport carried by an incoherent composite fluid, which we dub the an electron-phonon “soup”, characterized by an effective velocity $v_s < v_B < v_F$. We suggest that such behavior is ubiquitous in strongly interacting complex systems at high temperatures, and thus propose that it may explain much of the anomalous transport in “bad metallic” systems [e.g. catalogued by Bruin *et al.* [17], and discussed in terms of spectral weight transfer in [3, 4, 58]. Additional diffusivity measurements on these systems may test this proposal.

MATERIALS & METHODS

Samples

YBa₂Cu₃O_{6+y} single crystals were grown in non-reactive BaZrO₃ crucibles using a self-flux technique [59], with the Cu-O chains oxygen content accurately determined as described in Ref. [60]. The crystals used in our experiments were de-twinned. No twinning domains can be observed on the surface of the YBCO_{6.60} sample, and sparse thin strips of remnant domains can be seen on the YBCO_{6.75}, which were experimentally measured to have no effect on the measured diffusivity.

Diffusivity Measurements

For the high resolution thermal diffusivity measurements we use a home-built photothermal microscope [61, 62], described in details in the SI. The output power of a heating laser is modulated sinusoidally at a frequency $\omega \sim 1$ to 50 kHz, much smaller than typical electronic equilibration time [63], while a second laser measures the differential reflectivity at a fixed distance (r) from it. The diffusivity D is obtained by fitting the thermal phase delay ϕ between the source and the response signals as a function of frequency ω : $D = \omega r^2 / 2\phi^2$. Frequency sweeps at different distances yield consistent diffusivity values verifying the heat propagation model we used (for details see the SI).

Fits to Data

We use Eqn. 6 to fit the thermal diffusivity data. Literature values are used for the total specific heat [22], the electronic specific heat [56], Fermi velocity [57], and sound velocities [40, 64].

ACKNOWLEDGMENTS

We thank Subir Sachdev, Sam Lederer and Steve Kivelson for many insightful discussions. Work supported by the Gordon and Betty Moore Foundation through the EPiQS Initiative, Grant GBMF4529, and by a Department of Energy Early Career Award (SAH).

SIGNIFICANCE STATEMENT

Transport in the so-called “bad-metallic” regime of strongly correlated electron systems, with no well-defined electronic quasiparticles, has been a long-standing challenge in theoretical physics. This challenge has motivated the collection of an ample amount of data on bad metals.

However, so far emphasis has been given to the charge sector, with the host crystal lattice treated as a well-defined phonon background. In this paper we show that for the cuprates, in the bad-metallic regime where the resistivity exceeds the “Mott-Ioffe-Regel” limit, phonon excitations are also not well-defined. The data leads to a thermal transport scenario where entropy is carried by an overdamped diffusive fluid of electrons and phonons characterized by a unique velocity and a quantum-limited relaxation time $\hbar/k_B T$.

-
- [1] J.M. Ziman JM (1960) *Electrons and Phonons: The Theory of Transport Phenomena in Solids* (Oxford Univ Press, Oxford).
 - [2] Emery VJ, Kivelson SA (1995) Superconductivity in bad metals. *Phys Rev Lett* 74: 3253 - 3256.
 - [3] Gunnarsson O, Calandra M, Han JE (2003) Colloquium: Saturation of electrical resistivity. *Rev Mod Phys* 75:1085 - 1099.
 - [4] Hussey NE, Takenaka K, Takagi H (2004) Universality of the Mott-Ioffe-Regel limit in metals. *Philos Mag* 84:2847 - 2864.
 - [5] Slack GA (1979) The thermal conductivity of nonmetallic crystals. *Solid State Physics*, eds Ehrenreich H, Seitz F, Turnbull D (Academic, London), Vol 34, pp 1 - 71.
 - [6] Allen PB, Du XQ, Mihaly L, Forro L (1994) Thermal conductivity of Insulating Bi₂Sr₂YCu₂O₈ and superconducting Bi₂Sr₂CaCu₂O₈ - failure of the phonon-gas picture. *Phys Rev B* 49:9073 - 9079.
 - [7] Hartnoll SA (2015) Theory of universal incoherent metallic transport. *Nat Phys* 11:54 - 61.
 - [8] Norman MR, et al. (1998) Destruction of the fermi surface in underdoped high-Tc superconductors. *Nature* 392:157 - 160.
 - [9] Lanzara A, et al. (2001) Evidence for ubiquitous strong electron-phonon coupling in high-temperature superconductors. *Nature* 412:510 - 514.
 - [10] Segawa K, Ando Y (2001) Transport anomalies and the role of pseudogap in the 60-K phase of YBa₂Cu₃O_{6+δ}. *Phys Rev Lett* 86:4907 - 4910.
 - [11] Ando Y, Segawa K, Komiya S, Lavrov AN (2002) Electrical resistivity anisotropy from self-organized one dimensionality in high-temperature superconductors. *Phys Rev Lett* 88:137005.
 - [12] Le Boeuf D (2010) *Reconstruction de la surface de Fermi dans l'état normal d'un supraconducteur a haute Tc: Une etude du transport électrique en champ magnétique intense*. PhD thesis (Université de Sherbrooke, Sherbrooke, QC, Canada).
 - [13] Emin D (1992) Large-bipolaron transport and cuprate superconductors. *Phys Rev B* 45:5525 - 5529.
 - [14] Alexandrov AS, Mott NF (1994) Bipolarons. *Rep Prog Phys* 57:1197 - 1288.
 - [15] Sachdev S (1999) *Quantum Phase Transitions* (Cambridge Univ Press, Cambridge, UK), 1st Ed.
 - [16] Zaanen J (2004) Superconductivity: Why the temperature is high. *Nature* 430:512 - 513.
 - [17] Bruin JAN, Sakai H, Perry RS, Mackenzie AP (2013) Similarity of scattering rates in metals showing t-linear

- resistivity. *Science* 339:804 - 807.
- [18] Orenstein J, et al. (1990) Frequency- and temperature-dependent conductivity in $\text{YBa}_2\text{Cu}_3\text{O}_{6+x}$ crystals. *Phys Rev B* 42:6342 - 6362.
 - [19] Schlesinger Z, et al. (1990) Infrared studies of the superconducting energy gap and normal-state dynamics of the high- T_c superconductor $\text{YBa}_2\text{Cu}_3\text{O}_7$. *Phys Rev B* 41:11237 - 11259.
 - [20] Liu HL, et al. (1999) Doping-induced change of optical properties in underdoped cuprate superconductors. *J Phys Condens Matter* 11:239 - 264.
 - [21] van der Marel D, et al. (2003) Quantum critical behaviour in a high- T_c superconductor. *Nature* 425:271 - 274. Waske A, Hess C, Buechner B, Hinkov V, Lin CT (2007) Thermal conductivity of underdoped $\text{YBa}_2\text{Cu}_3\text{O}_y$. *Physica C Supercond* 460-462:746 - 747.
 - [22] Loram J, Mirza K, Freeman P (1990) The electronic specific heat of $\text{YBa}_2(\text{Cu}_{1-x}\text{Zn}_x)_3\text{O}_{6+\delta}$ from 1.6 K to 300 K. *Physica C Supercond* 171:243 - 256.
 - [23] Minami H, et al. (2003) Influence of the pseudogap on the thermal conductivity and the Lorenz number of $\text{YBa}_2\text{Cu}_3\text{O}_x$ above T_c . *Phys Rev B* 68:220503.
 - [24] Cyr-Choinière O, et al. (2015) Two types of nematicity in the phase diagram of the cuprate superconductor $\text{YBa}_2\text{Cu}_3\text{O}_y$. *Phys Rev B* 92:224502.
 - [25] Blanco-Canosa S, et al. (2014) Resonant x-ray scattering study of charge-density wave correlations in $\text{YBa}_2\text{Cu}_3\text{O}_{6+x}$. *Phys Rev B* 90:054513.
 - [26] Ghiringhelli G, et al. (2012) Long-range incommensurate charge fluctuations in $(\text{Y},\text{Nd})\text{Ba}_2\text{Cu}_3\text{O}_{6+\delta}$. *Science* 337:821 - 825.
 - [27] Achkar AJ, et al. (2012) Distinct charge orders in the planes and chains of ortho-iii ordered $\text{YBa}_2\text{Cu}_3\text{O}_{6+\delta}$ superconductors identified by resonant elastic x-ray scattering. *Phys Rev Lett* 109:167001.
 - [28] Bonnoit C, et al. (2012) Probing electronic order via coupling to low energy phonons in superconducting $\text{Bi}_2\text{Sr}_{2-x}\text{La}_x\text{CuO}_{6+\delta}$. *arXiv:1202.4994*.
 - [29] Le Tacon M, et al. (2014) Inelastic x-ray scattering in $\text{YBa}_2\text{Cu}_3\text{O}_{6.6}$ reveals giant phonon anomalies and elastic central peak due to charge-density-wave formation. *Nat Phys* 10:52 - 58.
 - [30] Parker W, Jenkins R, Abbott G, Butler C (1961) Flash method of determining thermal diffusivity, heat capacity, and thermal conductivity. *J Appl Phys* 32:1679 - 1684.
 - [31] Weast R, ed (1985) *CRC Handbook of Chemistry and Physics: A Ready-reference Book of Chemical and Physical Data*, (CRC, Boca Raton, FL), 66th Ed.
 - [32] Ekin J (2006) *Experimental Techniques for Low-temperature Measurements* (Oxford Univ Press, London).
 - [33] Yunus W, Fanny C, Moksini M, Phing T, Halim S (2001) Thermal diffusivity measurement of gold alloys and superconducting ceramics using photoacoustic technique. *Cleo/Pacific Rim 2001: The 4th Pacific Rim Conference on Lasers and Electro-Optics (IEEE, New York)*, pp 226 - 227.
 - [34] Hofmann F, et al. (2015) Non-contact measurement of thermal diffusivity in ionimplanted nuclear materials. *Sci Rep* 5:16042.
 - [35] Ang C, Chan S, Tan H (1974) Measurement of thermal diffusivity of mercury. *J Appl Phys* 45:179 - 181.
 - [36] Sundqvist B (1992) Thermal-diffusivity and thermal-conductivity of chromel, alumel, and constantan in the range 100-400-K. *J Appl Phys* 72:539 - 545.
 - [37] Sweet J, Roth E, Moss M (1987) Thermal-conductivity of Inconel-718 and 304 stainless steel. *Int J Thermophys* 8:593 - 606.
 - [38] Junod A, et al. (1987) Specific-heat of $\text{La}_{2-x}\text{Sr}_x\text{CuO}_4$ and $\text{YBa}_2\text{Cu}_3\text{O}_7$ superconductors from 1-K to room-temperature. *Jpn J Appl Phys* 26:1119 - 1120.
 - [39] Inyushkin A, Taldenkov A, Uvarova T (1996) Thermal conductivity of oxygen-deficient $\text{YBa}_2\text{Cu}_3\text{O}_{6+x}$. *Phys Rev B* 54:13261 - 13268.
 - [40] Lei M, et al. (1993) Elastic constants of a monocrystal of superconducting $\text{YBa}_2\text{Cu}_3\text{O}_{7-\delta}$. *Phys Rev B* 47:6154 - 6156.
 - [41] Junod A, et al. (1994) Specific heat up to 14 tesla and magnetization of a $\text{Bi}_2\text{Sr}_2\text{CaCu}_2\text{O}_8$ single-crystal thermodynamics of a 2d superconductor. *Physica C Supercond* 229:209 - 230.
 - [42] Nakamura Y, et al. (1991) Inplane and out of plane thermal conductivity of $\text{La}_{2-x}\text{Sr}_x\text{CuO}_4$ single crystals. *Physica C Supercond* 185:1409 - 1410.
 - [43] Ando Y, Boebinger GS, Passner A, Kimura T, Kishio K (1995) Logarithmic divergence of both in-plane and out-of-plane normal-state resistivities of superconducting $\text{La}_{2-x}\text{Sr}_x\text{CuO}_4$ in the zero-temperature limit. *Phys Rev Lett* 75:4662 - 4665.
 - [44] Sarrao J, et al. (1994) Complete elastic-moduli of $\text{La}_{2-x}\text{Sr}_x\text{CuO}_4$ ($x=0.00$ & 0.14) near the tetragonal-orthorhombic structural phase-transition. *Phys Rev B* 50:13125 - 13131.
 - [45] Wu X, et al. (1993) Thermal-diffusivity of $\text{Bi}_2\text{Sr}_2\text{CaCu}_2\text{O}_8$ single-crystals. *Physica C Supercond* 218:417 - 423.
 - [46] Fiamma R, Giura M, Sarti S, Marcon R, Silva E (2003) In-plane and out of plane resistivities in BSCCO (2212) single crystals at different doping level. *Int J Mod Phys B* 17:867 - 872.
 - [47] Triscone G, Junod A (1996) Thermal and magnetic properties. *Bismuth-Based High-Temperature Superconductors*, eds Maeda H, Togano K (CRC Press, Boca Raton, FL), p 33.
 - [48] Saunders G, et al. (1994) Anisotropy of the elastic and nonlinear acoustic properties of dense textured $\text{Bi}_2\text{Sr}_2\text{CaCu}_2\text{O}_{8+y}$. *Phys Rev B* 49:9862 - 9873.
 - [49] Gold Z, Gagnon R, Ellman B, Taillefer L, Behnia K (1994) Anisotropic thermalconductivity of $\text{YBa}_2\text{Cu}_3\text{O}_{7-\delta}$. *Physica C Supercond* 235:1485 - 1486.
 - [50] Deng X, et al. (2013) How bad metals turn good: Spectroscopic signatures of resilient quasiparticles. *Phys Rev Lett* 110:086401.
 - [51] Reeves ME, Ditmars DA, Wolf SA, Vanderah TA, Kresin VZ (1993) Evidence for strong electron-phonon coupling from the specific heat of $\text{YBa}_2\text{Cu}_3\text{O}_{7-\delta}$. *Phys Rev B* 47:6065 - 6068.
 - [52] Zhang Y, et al. (2000) Determining the Wiedemann-Franz ratio from the thermal hall conductivity: Application to Cu and $\text{YBa}_2\text{Cu}_3\text{O}_{6.95}$. *Phys Rev Lett* 84:2219 - 2222.
 - [53] Blake M (2016) Universal charge diffusion and the Butterfly effect. *Phys Rev Lett* 117:091601.
 - [54] Shenker SH, Stanford D (2014) Black holes and the butterfly effect. *J High Energy Phys* 03:067.
 - [55] Roberts DA, Stanford D, Susskind L (2015) Localized shocks. *J High Energy Phys* 03:051.

- [56] Moler KA, et al. (1997) Specific heat of $\text{YBa}_2\text{Cu}_3\text{O}_{7-\delta}$. Phys Rev B 55:3954 - 3965.
- [57] Fournier D, et al. (2010) Loss of nodal quasiparticle integrity in underdoped $\text{YBa}_2\text{Cu}_3\text{O}_{6+x}$. Nat Phys 6:905 - 911.
- [58] Jaramillo R, Ha SD, Silevitch DM, Ramanathan S (2014) Origins of bad-metal conductivity and the insulator-metal transition in the rare-earth nickelates. Nat Phys 10:304 - 307.
- [59] Liang R, Bonn D, Hardy W (1998) Growth of high quality YBCO single crystals using BaZrO_3 crucibles. Physica C Supercond 304:105 - 111.
- [60] Liang R, Bonn DA, Hardy WN (2006) Evaluation of CuO_2 plane hole doping in $\text{YBa}_2\text{Cu}_3\text{O}_{6+x}$ single crystals. Phys Rev B 73:180505.
- [61] Fanton JT (1990) Analysis and applications of photothermal microscopy. PhD thesis (Stanford University, Stanford, CA).
- [62] Wu XD, Kino GS, Fanton JT, Kapitulnik A (1993) Photothermal microscope for high-Tc superconductors and charge density waves. Rev Sci Instrum 64:3321 - 3327.
- [63] Li W, Zhang C, Wang X, Chakhalian J, Xiao M (2015) Ultrafast spectroscopy of quasiparticle dynamics in cuprate superconductors. J Magn Magn Mater 376:29 - 39.
- [64] Shekhter A, et al. (2013) Bounding the pseudogap with a line of phase transitions in $\text{YBa}_2\text{Cu}_3\text{O}_{6+\delta}$. Nature 498:75 - 77.

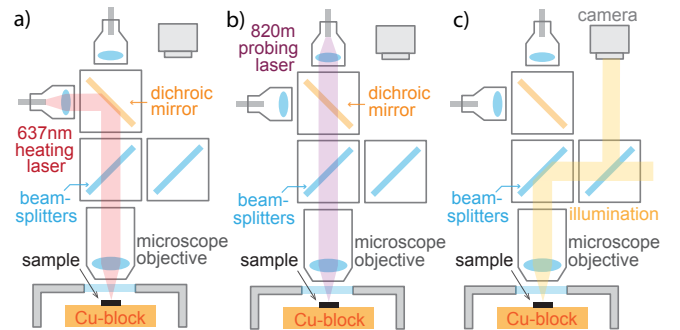
SUPPORTING INFORMATION (SI)

Samples

$\text{YBa}_2\text{Cu}_3\text{O}_{6+y}$ single crystals were grown in non-reactive BaZrO_3 crucibles using a self-flux technique [59], with the Cu-O chains oxygen content accurately determined as described in Ref: [60]. The CuO-chain oxygen content was set to $y = 6.60, 6.67$, and 6.75 by annealing in a flowing $\text{O}_2:\text{N}_2$ mixture and homogenized by further annealing in a sealed quartz ampoule, together with ceramic at the same oxygen content. The absolute oxygen content (y) is accurate to ± 0.01 based on iodometric titration. The crystals used in our experiments were detwinned. No twinning domains can be observed on the surface of the $\text{YBCO}_{6.60}$ sample, and sparse thin strips of remnant domains can be seen on the $\text{YBCO}_{6.75}$, which were experimentally measured to have no effect on the measured diffusivity.

Principles of the Photothermal Apparatus

For the high resolution thermal diffusivity measurements we use a home-built photothermal microscope [61, 62]. The microscope views the sample through a sapphire optical window in a cryostat, with the sample mounted to a cold finger just under the window. A schematic is shown in Fig. S1. A heating laser at 637 nm and a probing laser at 820 nm are focused onto the sample surface by the microscope objective. The focused spots have Gaussian radii of approximately $1\mu\text{m}$ and $2\mu\text{m}$, respectively, due to the diffraction limit of the different wavelengths, and can be moved independently over the sample surface. A camera allows us to align the spots and observe the sample surface nearby. Fig.S 2 shows a

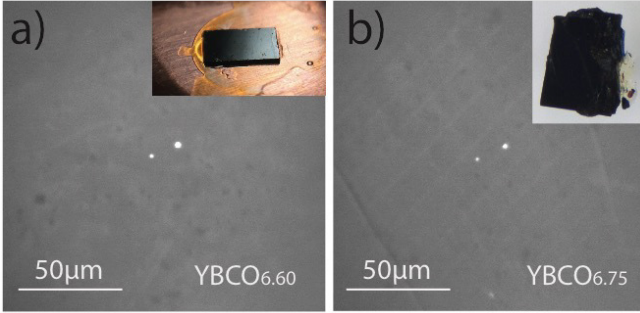


S 1. (color online) The schematic shows the optical paths of the setup. (a) Path of the heating laser (b) Path of the probing laser. The reflected light traverse the same path before gathered by a photodetector. (c) Path of camera vision. Cross-polarized picture is obtained by polarizing the incoming illumination and placing an analyzer in front of the camera.

camera view of the two beams on different surfaces that

we examined.

The output power of the heating laser is modulated with a sinusoidal profile $P(t) = P_0[1 + \sin(\omega_0 t)]$. The modulation frequency $\omega_0/2\pi$ has a typical range of 1 kHz - 50 kHz, much slower than the microscopic equilibration time which is on the order of picoseconds [63]. This means that the parameters extracted are all within the in the DC limit of linear response, and are independent of the modulation frequency itself. The probing laser is aimed at a spot a small distance (typically 10 – 20 μm) away from the heating laser. The reflected light from the probing laser is diverted by an optical circulator and fed into a photodetector. The AC component of the photodetector signal is then fed to a lock-in amplifier referenced to the laser modulation and the amplitude and phase are measured. The large differential reflectivity dR/dT of the YBCO samples (about $10^{-5} - 10^{-6} \text{ K}^{-1}$) at the wavelength of the probe light allows us to study their thermal properties with minimal disturbance.



S 2. (color online) Cross-polarized image of the samples showing both laser spots: left (smaller spot) is the 637nm heating spot and right (larger spot) is the 830nm probe laser spot. a) a typical area of single crystal detwinned YBCO_{6.60}, and b) a typical area of single crystal detwinned YBCO_{6.75}. Thin remnant strips of the opposite structural domain is visible as white lines, but have been shown to have negligible effect on the anisotropy measurements. Insets show pictures of the crystals measured.

Measuring Thermal Diffusivity

The diffusive transport of heat is governed by the diffusion equation

$$\frac{\partial \delta T(t, \vec{r})}{\partial t} - D \nabla^2 \delta T(t, \vec{r}) = \frac{q(t, \vec{r})}{c} \quad (8)$$

where δT is the temperature disturbance above the ambient temperature T , $\vec{r} = \{x_1, x_2, x_3\}$ is the spherical radial coordinate given in terms of the euclidean principal axes x_i , q is the absorbed power density, c is the volumetric specific heat capacity, $D \equiv \kappa/c$ is the thermal diffusivity, and κ is the thermal conductivity. Note that c and D are themselves functions of T , but in the

limit of weak heating $\delta T \ll T$, we make the approximation $c(T + \delta T) \approx c(T)$ and $D(T + \delta T) \approx D(T)$. As mentioned in the main text, the temperature disturbance from both lasers is $\lesssim 1 \text{ K}$ through out the temperature range 25 ~ 300 K, so this approximation is valid.

The modulated power of the heating laser causes ripples in the temperature profile at the sample surface, which may be measured by the probing laser. It is useful to write the response in frequency space $\delta \tilde{T}(\omega, \vec{r})$, where

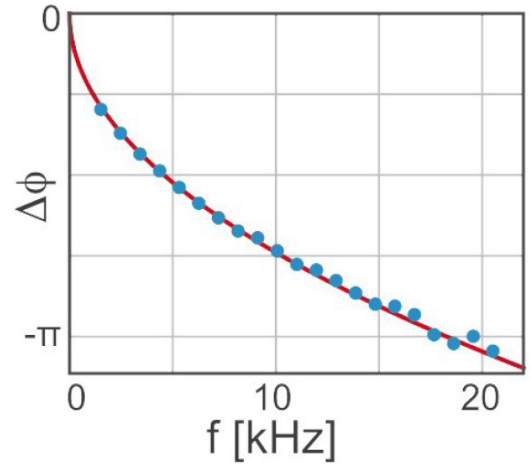
$$\delta T(t, \vec{r}) = \int \delta \tilde{T}(\omega, \vec{r}) \exp(-i\omega t) d\omega \quad (9)$$

We model the focused heat source as a point source, $q(t, \vec{r}) = P_0 e^{-i\omega t} \delta^3(\vec{r})$. This approximation is valid as long as the distance from the heating spot is much larger than the spot radius. In a semi-infinite isotropic system, the temperature profile is spherically symmetric and takes the form

$$\delta \tilde{T}(\omega, r) = \underbrace{\frac{P_0}{\kappa} \frac{1}{r} \exp\left(-\sqrt{\frac{\omega}{2D}} r\right)}_{\text{amplitude}} \underbrace{\exp\left(-i\sqrt{\frac{\omega}{2D}} r\right)}_{\text{phase}} \quad (10)$$

Our measurement gives us the response at the modulation frequency ω_0 .

Although both the amplitude and the phase of the solution carry information about D , in actual measurements factors such as mechanical vibrations, fluctuations in the laser power, and the temperature dependence of the differential reflectivity dR/dT affect the amplitude of the reflectivity oscillation. These factors do not affect the phase of the signal, which is therefore the more robust probe. We obtain D by fitting the phase delay ϕ between the source and the response signals as a function of ω at fixed r : $D = \omega r^2 / 2\phi^2$. A typical fit is shown in Fig.S 3. It is important to note that frequency sweeps at different



S 3. (color online) Typical phase delay data (blue circles) obtained by sweeping modulation frequency. The red line is a fit using the form in Eq. 10.

distances yield consistent diffusivity values verifying the assumptions we used in obtaining the ideal solution.

Anisotropic Diffusion Equation

A general system may be anisotropic, but can be reduced to the isotropic case through a change of variables. To begin, we write down the heat diffusion equation for a generic system,

$$\frac{\partial \delta T(t, \vec{r})}{\partial t} - D_{ij} \nabla_i \nabla_j \delta T(t, \vec{r}) = \frac{q(t, \vec{r})}{c} \quad (11)$$

It is interesting to note that the dimension of the diffusivity consists only of space and time: $[D] = \text{cm}^2/\text{s}$. A coordinate-isotropic solution can always be found through spatial rotation and scaling. Starting from the diagonal coordinates of the diffusivity tensor,

$$\sum_{ij} D_{ij} \nabla_i \nabla_j = \sum_i D_i \frac{\partial^2}{\partial x_i^2} = D_1 \sum_i \frac{\partial^2}{\partial z_i^2} = D_1 \tilde{\nabla}^2 \quad (12)$$

where we choose to keep the first axis untouched, and scale the rest accordingly, $z_i = x_i \sqrt{D_1/D_i}$. In the new coordinates, diffusion is an isotropic process, and diffusivity is characterized by a single number. In this new set of coordinate \vec{z} , the absorbed power density transforms accordingly as,

$$q(t, \vec{z}) = P_0 \sqrt{\frac{D_1^2}{D_2 D_3}} e^{-i\omega t} \delta^3(\vec{z}).$$

We now want to recover the anisotropic dependence on D_{ij} on the surface of the sample in the original coordinate. Let $x_3 = z_3 = 0$ on the surface, let (ρ, θ) be the original polar coordinate on the surface

$$r^2 = z_1^2 + z_2^2 = x_1^2 + \frac{D_1}{D_2} x_2^2 = \rho^2 (\cos^2 \theta + \frac{D_1}{D_2} \sin^2 \theta) \quad (13)$$

This leads to the exponent in Eqn. 10 being rescaled as

$$\sqrt{\frac{\omega}{2D}} r = \sqrt{\frac{\omega}{2} \frac{D_2 \cos^2 \theta + D_1 \sin^2 \theta}{D_1 D_2}} \rho \quad (14)$$

which leads to the extracted diffusivity

$$D = \frac{D_1 D_2}{D_2 \cos^2 \theta + D_1 \sin^2 \theta} \quad (15)$$

Alignments and Data Collection

To check the alignment confirm the orientation of the sample, we first measure diffusivity as a function of frequency for different orientations around the heating spot. This is typically done at room temperature and frequency

sweeps are typically between 500 Hz and 20 kHz. For each orientation we generate a set of data similar to that shown in Fig. S3, and from the fit extract the diffusivity $D(\theta)$. We then performed an overall fit of Eq. 15 to all sets of frequency sweeps at various sample orientations, where an additional offset angle is left as an additional free parameter. This offset is the difference between the arbitrary initial angle that we used and the actual principal directions of the crystal. All offset angles are later verified to align with the crystal edge within statistical uncertainties. Typical fits are shown in the insets of Fig. 1 of the main manuscript. We note that error bars are almost entirely due to an uncertainty of $\sim 0.5 \mu\text{m}$ in determining laser spots separation due to their finite spread. Excellent fit to the functional form Eq. 12 is obtained on both samples (see main text), including in the region on YBCO_{6.75} crystal with thin stripes of remnant domains, Fig. S2(b), verifying the anisotropic diffusivity measurements are effectively single-domain in nature.

The temperature dependent diffusivity on each axis is then taken by continuously vary the temperature at a fixed laser separation on each axis, at a fixed modulation frequency ($\sim 20\text{kHz}$), and at the same region where the room temperature anisotropy has been measured.

Fits to the Electron-Phonon “Soup” Model

We fit the thermal diffusivity measurement of the three YBCO_{6+x} samples using the form

$$D = \frac{\hbar}{2k_B T} \left(\alpha_e \frac{c_e(T)}{c(T)} v_F^2 + \alpha_{ph} \frac{c_{ph}(T)}{c(T)} v_s(T)^2 \right), \quad (16)$$

where literature values are used for the total heat capacity c [22], the electronic heat capacity c_e [56], Fermi velocity v_F [57], and sound velocities[40, 64]. The following table lists the coefficients α_e and α_{ph} in the plane (a) and chain (b) directions as extracted from the fits, with their standard errors:

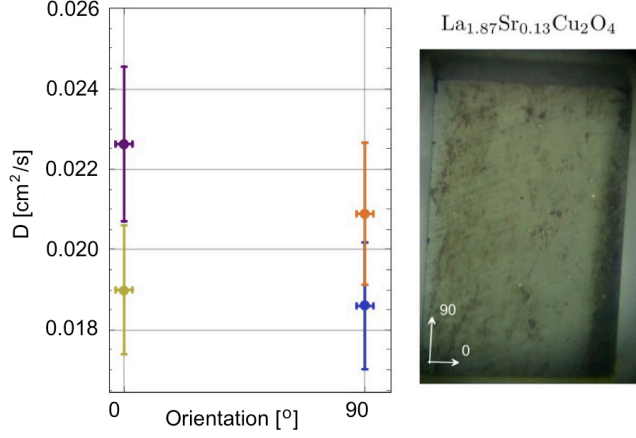
Table II. Results for fitting constants in equation 16

	α_e	α_{ph}
YBCO _{6.60} plane	0.14 ± 0.01	2.0 ± 0.1
chain	0.413 ± 0.007	2.58 ± 0.06
YBCO _{6.67} plane	0.13 ± 0.02	2.1 ± 0.3
chain	0.34 ± 0.06	2.6 ± 0.5
YBCO _{6.75} plane	0.25 ± 0.02	1.64 ± 0.09
chain	0.53 ± 0.02	2.82 ± 0.2

Preliminary Measurements on LSCO

To complete the diffusivity data that we present in Table 1 of the main text, we measured the thermal diffusivity on a $\sim 1 \times 2 \times 0.8 \text{ mm}^3$ La_{2-x}Sr_xCu₂O₄ ($x = 0.13$)

single crystal. In Fig. S4 we show preliminary results of room-temperature measurements, together with a picture of the crystal. While the surface of the crystal was scratched, high-quality data could be obtained in high reflectivity regions. As expected, no obvious anisotropy was detected.



S 4. (color online) Left: Typical data in two perpendicular orientations measured on a $\text{La}_{1.87}\text{Sr}_{0.13}\text{Cu}_2\text{O}_4$ single crystal. Right: a picture of the surface of the crystal measured.